A hierarchical multi-scale analytical approach for predicting the elastic behavior of short fiber reinforced polymers under triaxial and flexural loading conditions

H. Ahmadi[1, 2 *], M. Hajikazemi[1, 3], E. Rashidinejad[1], Y. Sinchuk[1], W. Van Paepegem[1]

[1] Department of Materials, Textiles and Chemical Engineering, Faculty of Engineering and Architecture, Ghent University, Technologiepark Zwijnaarde 46, Ghent, Belgium

[2] SIM Program M3 ProPel, Technologiepark 48, Zwijnaarde B-9052, Belgium

[3] Dutch Polymer Institute (DPI), P.O. Box 902, 5600 AX, Eindhoven, Netherlands

Abstract

This paper presents a computationally efficient multi-scale analytical framework for predicting the effective elastic response of short fiber reinforced polymers (SFRPs) under triaxial and flexural loading conditions where the details of microstructure such as core/shell thickness, volume fraction distribution, fiber misalignment and fiber length variation are objectively taken into account. To this end, the mean-field homogenization and finite element approaches are compared to calculate the elastic response of SFRPs at the microscopic level while the orientation averaging approach is used to address the effects of fiber misalignment. The obtained mechanical behavior is then linked to an enhanced laminate theory to predict the effective triaxial and bending macrostructural behavior considering the core/shell effects and variation of volume fraction through the thickness. Using the second-order homogenization technique, the numerical validation of the proposed analytical approach is investigated based on the micro- and meso-scale analyses. Furthermore, the potential of the proposed strategy is demonstrated for hybrid composites. Finally, the accuracy of the suggested model is thoroughly studied using the available experimental tests in literature where the statistical information about the details of SFRP microstructures is presented.

Keywords: Short fiber reinforced polymers, Core/shell effect, Volume fraction distribution, Periodic boundary conditions (PBCs), Out-of-plane and flexural properties

1. Introduction:

Short fiber reinforced polymers (SFRPs) are attracting considerable attention of various industrial sectors due to the fast and low-cost manufacturing processes and interesting mechanical properties [1, 2]. Short fiber composites are mainly produced by the injection molding process and have complex microstructures [3, 4]. One key step in the design of SFRPs is the prediction of effective mechanical behavior at the macroscopic level. However, the microstructural complexities such as core-shell effects, fiber orientation/length and volume fraction distributions bring difficulties in estimating the effective mechanical response of SFRPs. Therefore, considering the effects of microstructural details in the analysis,

*Corresponding Author, E-mail address: Hossein.Ahmadi@UGent.be, Postal address: Technologiepark 46, 9052 Zwijnaarde, Ghent, Belgium.

more specifically the distribution of fiber orientation and volume fraction through the thickness, is an essential step for reliable prediction of the triaxial and flexural mechanical performance of SFRPs.

Finite element approach as a powerful numerical tool [5-7] has been frequently used to estimate the mechanical response of SFRPs in a wide range of domains [8-17]. In this regard, Breuer and Stommel [18] studied the effects of fiber geometry, packing configuration, fiber length and orientation distributions on the elastic response of SFRPs. Also, Tian et al. [19] focused on the Representative Volume Element (RVE) generation for SFRPs with randomly distributed fibers and high volume fractions at the microscale level. It should be noted that the RVE generation and FE meshing are challenging tasks for FE modeling of SFRPs and it is very difficult and time-consuming to generate and analyze RVEs with adequate finite element meshing. Consequently, different numerical studies predicted the effects of fiber misalignment using Pseudo-grain and averaging approaches. Naili et al. [20] utilized 2D finite element (FE) simulations to obtain the mechanical response of SFRPs with a distribution of fiber orientations based on different orientation averaging approaches. Similarly, Mirkhalaf et al. [21] employed the FE-based orientation averaging to estimate the elastic response of misaligned SFRPs composites in the three-dimensional domain. A pseudo-grain approach was developed by Pietrogrande et al. [19] to explore the elastic stress distributions in the matrix for misaligned SFRPs based on the information obtained from aligned RVEs. In the above mentioned studies, there is always a need of finite element simulations for predicting the elastic behavior of aligned unit-cells/RVEs to estimate the elastic response of RVEs with misaligned fibers using orientation averaging approaches. Although the FE simulation is powerful for estimating the mechanical response of SFRPs in different length scales, it is practically limited by very high computational costs.

The mean-field homogenization can be used as an alternative approach for estimating the mechanical response of SFRPs with acceptable accuracy and very low computational costs compared to the numerical solutions. Among various mean-field homogenization (MFH) techniques, the Mori-Tanaka approach [22, 23] is well-known for predicting the elastic response of aligned SFRPs. This method has been extensively used to predict the mechanical behavior of composite materials [24-29]. By comparing the elastic response obtained from different analytical solutions such as Mori–Tanaka [22, 23], self-consistent model [30, 31], Halpin–Tsai [32], bounding [33, 34] and shear lag [35] models with the finite element simulation, Tucker and Liang [36] demonstrated that the Mori-Tanaka approach can provide good predictions for the elastic response of unidirectional short-fiber composites. Also, Pierard et al. [24] provided a general framework for predicting the thermo-elastic behavior of multi-phase composite materials using MFH approaches and two-step homogenization approaches. Dray et al. [37] investigated the use of different Closure approaches in the mean-field homogenization (Mori-Tanaka) to predict the effects of misalignment in the effective thermo-elastic behavior of SFRPs. They recognized that a fitted closure approach leads to the best prediction for the elastic response of SFRPs

with misaligned fibers. Additionally, Jain et al. [15, 38] indicated that the average stress responses of the inclusions with 2D planar distribution can be easily predicted by using Pseudo-grain and Mori-Tanaka approaches.

Most of the available analytical and numerical studies have focused only on the mechanical response of SFRPs with a single-layer model (misaligned/aligned). However, several microscopic observations and x-ray scans reveal that the orientation distribution of the fibers and the volume fraction are varying through the thickness [39]. Considering the variation of microstructural details through the thickness is vital specially when out-of-plane and bending properties are concerned. To deal with these effects, decomposing the SFRP thickness into several layers can be a possible solution. In this case, the SFRPs structures can be assumed as a laminate with several plies where the effects of local fiber orientation and volume fraction are considered in each ply. There exists also another strategy where the through-thickness average orientation tensor and volume fraction of the SFRPs can be used for obtaining the mechanical response [21, 40]. Nevertheless, this method cannot be trusted for predicting the flexural behavior of SFRP and has less accuracy in estimating the in-plane and out-of-plane effective properties. In addition, there are several applications for hybrid composites where SFRPs are combined with other composite systems such as overmoulding of unidirectional continuous fiber laminates or particulate composites [41-43]. Thus, it is important to couple the microscopic information of SFRPs to three-dimensional enhanced laminate theories to be able to predict complete mechanical response (in-plane, out-of-plane and bending) with limited computational cost.

Only a limited number of researchers considered the classical laminate theory for SFRPs. For example, Halpin and Kardos [44] utilized 0°, 90° and ±45° aligned plies of SFRPs in the classical laminate theory to construct a quasi-isotropic laminate as a 2D SFRP. Also, Shokrieh and Moshrefzadeh-Sani [45] used the laminate analogy for the in-plane SFRPs with misaligned fibers where an equivalent laminated composite with several unidirectional plies was used to predict the progressive damage in SFRPs based on shear-lag, Halpin-Tsai and Tsai-Wu failure criteria. It should be noted that the mentioned studies were all restricted to the two-dimensional analyses and the laminate theory was used only for averaging the orientation distribution of fibers. Moreover, few studies have been carried out on the flexural response of SFRPs and hybrid composites using analytical approaches. Fu et al. [46] utilized a 2D analytical solution for predicting the flexural behavior of SFRPs. The study ignores the variation of volume fraction through the thickness and also neglects the effects of out-of-plane deformation on the mechanical behavior of composite materials. Moreover, a simplified orientation averaging approach was employed to consider the effects of 2D fiber misalignment for a laminate with only three plies (core and shell). As we will show in this paper, the implementation of laminate analogy for estimating the triaxial and bending deformation of SFRPs involves different modeling ingredients. Therefore, the accuracy of the laminate analogy for SFRPs must be examined numerically step by step. Experimental validation of laminate analogy specially under complex bending deformations is cumbersome as the presence of possible non-linear

effects and the assumptions involved for different modeling steps might compensate each other. Therefore, it is important to use the finite element simulations for complex loading conditions and provide benchmark solutions for different modeling ingredients in the micro- and meso-scale levels.

The main contribution of this study is linking the Mori-Tanaka approach to a three-dimensional enhanced laminate theory in order to predict the triaxial and flexural effective elastic properties of SFRPs and hybrid composite materials. The proposed strategy can then consider the variation of microstructural details such as volume fraction and orientation tensor through the thickness. In order to validate the different modeling ingredients, highly refined FEM simulations at micro- and meso-scales are performed incorporating second-order periodic boundary conditions. To do so, the second-order periodic boundary conditions are enhanced to include the effects of out-of-plane deformations. Moreover, different existing orientation averaging approaches have been employed for both numerical and analytical homogenization methods. The aim and novelty of this study can be summarized as follows:

- Suggesting a hierarchical multi-scale analytical framework to predict the effective behavior of SFRPs and hybrid composites.
- Linking the mean-field homogenization technique and microscale FE modeling (for validation) to the enhanced classical laminate theory to predict all the triaxial and bending properties.
- Coupling second-order homogenization technique to a three-dimensional enhanced laminate theory in order to obtain the effective triaxial [$\boldsymbol{A}$], coupling [$\boldsymbol{B}$] and bending [$\boldsymbol{D}$] stiffness matrices of SFRP composites with $(7 * 7)$ components.
- Using second-order homogenization formulations in FEM modeling of SFRPs and hybrid RVEs in micro and mesoscale levels to verify the assumptions of laminate analogy for SFRPs.
- Providing benchmark solutions for the flexural behavior of SFRPs and hybrid composite materials in different length scales using analytical and numerical models.
- Experimental validation of the modeling results by comparison to the high-quality DIC measurements on the SFRP samples in the presence of corresponding accurate information about microstructural details obtained from CT images

2. Methodologies

In this section, the details of the required analytical and numerical approaches for multiscale modeling of SFRPs are presented. Fig. 1 demonstrates the required steps for the proposed multi-scale strategy. As illustrated, the Mori-Tanaka mean-field homogenization or finite element approaches are considered to capture the elastic response of aligned SFRPs in the microscale analysis. By linking the obtained mechanical response to the Pseudo-grain/Closure approach, the effects of fiber misalignment are taken into account. Then, the homogenized elastic behavior of misaligned fiber is

utilized as a material property of each ply in the three-dimensional enhanced laminate theory or FEM modeling with second-order homogenization formulations. In this case, the through-thickness variation of volume fraction and core/shell effects can be easily considered. It is noted that finite element modeling with a second-order homogenization approach is performed to indicate the accuracy of the suggested multi-scale analytical modeling under a variety of loading conditions.

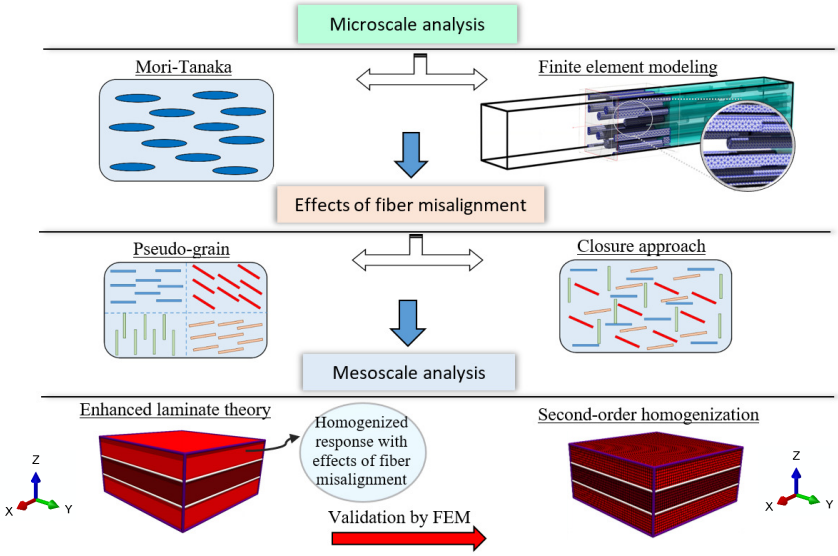

Figure 1. Schematic description of coupling the mesoscale analysis with the microscopic information.

In this study, the mechanical behavior of microstructures is considered as linear elastic and the effects of thermal or moisture residual stress are ignored. Moreover, the global coordinate system (X, Y and Z) is selected to report the mechanical properties of composite materials (Fig. 1).

2.1. Micro-mechanical analysis

2.1.1. Analytical solution for aligned short fiber composites

The Mori-Tanaka model is an efficient homogenization approach for exploring the mechanical response of different composite materials based on the average stress and strain response in the matrix and inclusions. This method was proposed by Mori and Tanaka [22] and reformulated by Benveniste [23] to compute the total stiffness tensor for composite materials with different shapes of inclusions such as ellipsoidal, spherical, infinite cylinder, and penny-shaped disc. This approach relies on Eshelby's equivalent inclusion problem which is developed for solving the stress field of an ellipsoidal inclusion in an infinite elastic domain. Moreover, the Mori-Tanaka scheme can approximate the interactions between the inclusions by a modification of the applied strain to each inclusion in the strain concentration tensor [23].

The effective stiffness tensor of a two-phase composite material can be expressed in the following form

$$\overline{\boldsymbol{C}} = \vartheta_m \boldsymbol{C}_m : \boldsymbol{A}_m + \vartheta_i \boldsymbol{C}_i : \boldsymbol{A}_i \,, \tag{1}$$

where ϑ, $\boldsymbol{C}$ and $\boldsymbol{A}$ represent the volume fraction, the stiffness and the strain concentration tensor for each phase, respectively. The subscript *m* and *i* refer, respectively, to the matrix and inclusion phases. The strain concentration tensor is mainly correlating the applied strain ε to the average strain components of each phase (denoted by $\boldsymbol{\varepsilon_i}$ and $\boldsymbol{\varepsilon}_m$) and the relation between the strain concentration tensors can be defined as

$$\boldsymbol{\varepsilon}_i = \boldsymbol{A}_i : \boldsymbol{\varepsilon} \,, \tag{2}$$

$$\boldsymbol{\varepsilon}_m = \boldsymbol{A}_m : \boldsymbol{\varepsilon} \,, \tag{3}$$

$$\boldsymbol{I} = \boldsymbol{A}_m + \boldsymbol{A}_i \,, \tag{4}$$

where $\boldsymbol{I}$ denotes the symmetric identity tensor. Equation (1) can be presented in a simpler form based on the strain concentration of the inclusion as

$$\overline{\boldsymbol{C}} = \boldsymbol{C}_m + \vartheta_i(\boldsymbol{C}_i - \boldsymbol{C}_m) : \boldsymbol{A}_i \,. \tag{5}$$

Using the dilute strain concentration of the inclusion, the strain concentration tensor of Mori-Tanaka $\boldsymbol{A}_i^{MT}$ can be determined by the following equations

$$\boldsymbol{A}_i^{Dilute} = [\boldsymbol{I} + \boldsymbol{S}_E : \boldsymbol{C}_m^{-1} : (\boldsymbol{C}_i - \boldsymbol{C}_m)]^{-1} \,, \tag{6}$$

$$\boldsymbol{A}_i^{MT} = \boldsymbol{A}_i^{Dilute} : [\vartheta_m \boldsymbol{I} + \vartheta_i \boldsymbol{A}_i^{Dilute}]^{-1} \,, \tag{7}$$

where $\boldsymbol{S}_E$ is the Eshelby tensor which only depends on the aspect ratio of the inclusion and the Poisson's ratio of the matrix. The readers can find the components of the Eshelby tensor in Ref. [47, 48].

Using equation (5) and equation (6), it is possible to predict the total stiffness tensor of the composite and extract the compliance tensor $\bar{S}$ as

$$\overline{\boldsymbol{S}} = \overline{\boldsymbol{C}}^{-1} \,. \tag{8}$$

Therefore, it would be possible to extract the effective elastic constants based on the components of the compliance tensor $\overline{\boldsymbol{S}}$ as follows

$$E_{xx} = \frac{1}{\bar{s}_{11}}, E_{yy} = \frac{1}{\bar{s}_{22}}, E_{zz} = \frac{1}{\bar{s}_{33}}, \nu_{xy} = -\frac{\bar{s}_{12}}{\bar{s}_{11}}, \nu_{xz} = -\frac{\bar{s}_{13}}{\bar{s}_{11}}, \nu_{yz} = -\frac{\bar{s}_{23}}{\bar{s}_{22}}, G_{xy} = \frac{1}{\bar{s}_{66}}, G_{xz} = \frac{1}{\bar{s}_{55}}, G_{yz} = \frac{1}{\bar{s}_{44}}, \tag{9}$$

where E, ν and G are respectively Young's modulus, Poisson's ratio and shear modulus. The (X, Y and Z) represent the directions in the global coordinate system.

2.1.2. Numerical approach for aligned short fiber composites

As an alternative to analytical solutions, finite element modeling with periodic boundary conditions (PBCs) can be performed to extract the mechanical response of the composite at the microscopic level. The 3D periodic boundary

conditions (PBCs) is one of the most effective approaches for reducing the computational cost while evaluating the homogenized behavior of composite materials in various length scales [49, 50]. Based on this approach the nodal displacements fields of opposite surfaces can be correlated to each other using a linear equation which can be expressed as [51]

$$u_j^{i+} - u_j^{i-} = \varepsilon_{ij} l_i \quad (i,j = x,y,z)\,, \tag{10}$$

where u and l_i are, respectively, the displacement fields for opposite nodes and the length of RVE in the *i* direction. In order to extract the homogenized response of the composite material, the average stress and strain response can be obtained using the information from the reference points or data at the integration points of the whole RVEs which is given as

$$\bar{\sigma}_{ij} = \frac{1}{V}\int_V \sigma_{ij} dV, \tag{11}$$

$$\bar{\varepsilon}_{ij} = \frac{1}{V}\int_V \varepsilon_{ij} dV. \tag{12}$$

Six loading conditions with unit values (three uniaxial loads in X, Y and Z and three shear loads in X-Y, X-Y and Y-Z directions) are required to compute all the elastic constants of composite materials [5]. The elastic constants can then be extracted from equations (8) and (9) by having the stiffness tensor from Hooke's law as

$$\bar{\boldsymbol{\sigma}} = \bar{\boldsymbol{C}}\bar{\boldsymbol{\varepsilon}}\,. \tag{13}$$

In the current work, for applying the PBCs and post-processing the results, Python scripts are utilized in the Abaqus finite element software [52].

2.2. Orientation averaging

It is well-known that the RVE generation for non-aligned SFRPs is very cumbersome [19]. In addition to the high computational costs, many issues stand in the way such as meshing problems and difficulty in RVE generation for high fiber volume fractions [21]. These problems can be approximately solved using the Pseudo-grain/Closure approach [20, 27, 53].

The orientation tensor provides computationally efficient information about the status of fiber orientation in 3D and 2D spaces where this data can be used for considering the effects of fiber misalignment in the mechanical behavior of SFRPs.

The unit vector $\boldsymbol{p}$, which depends on (θ, φ), can be used to describe the orientation of a single fiber in a 3D configuration. As can be seen in Fig. 2, φ and θ represent, respectively, the in-plane and out-of-plane orientations of a single fiber based on the defined coordinate system. The X'_1, X'_2 and X'_3, respectively, refer to the fiber direction, in-plane transverse and out-of-plane transverse directions to the fiber in the local coordinate system.

$$\boldsymbol{p} = \begin{bmatrix} p_1 \\ p_2 \\ p_3 \end{bmatrix} = \begin{bmatrix} \sin\theta\cos\varphi \\ sin\,\theta\,sin\,\varphi \\ \cos\theta \end{bmatrix}. \tag{14}$$

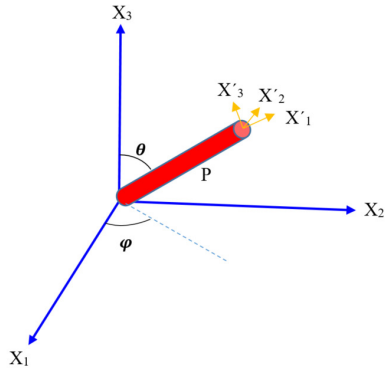

Figure 2. Demonstration of fiber orientation vector in a three-dimensional coordinate system (X_1, X_2, X_3).

The probability orientation distribution function $\psi(\theta,\varphi)$ can be used to represent the orientation state of a point in space. This function $\psi(\theta,\varphi)$ implies the probability to find fiber in the orientation between (θ, φ) and ($\theta+d\theta$, $\varphi+d\varphi$) which is denoted by[54]:

$$P(\theta_1 \le \theta \le \theta_1 + d\theta, \varphi_1 \le \varphi \le \varphi_1 + d\varphi) = \psi(\theta_1,\varphi_1)\sin\theta_1\, d\varphi\, d\theta \tag{15}$$

The orientation distribution function $\psi(\theta,\varphi)$ satisfies the following physical conditions

$$\int_{\varphi=0}^{2\pi}\int_{\theta=0}^{2\pi}\psi(\theta,\varphi)\, sin\,\theta\, d\varphi\, d\theta = \oint\psi(\boldsymbol{p})d\boldsymbol{p} = 1 \text{ (normalization condition)}, \tag{16}$$

$$\psi(\theta,\varphi) = \psi(\pi-\theta,\pi+\varphi)\ or\ \psi(\boldsymbol{p}) = \psi(-\boldsymbol{p}) \text{ (symmetry of the fiber)}. \tag{17}$$

Using the unit vector of fiber $\boldsymbol{p}$ and the orientation distribution function $\psi(\boldsymbol{p})$ for each possible direction, the second-order and fourth-order orientation tensors (a_{ij} and a_{ijkl}) can be defined as [54]:

$$a_{ij} = \oint p_i p_j \psi(\boldsymbol{p}) d\boldsymbol{p}\ , \tag{18}$$

$$a_{ijkl} = \oint p_i p_j p_k p_l \psi(\boldsymbol{p}) d\boldsymbol{p}\ , \tag{19}$$

$$d\boldsymbol{p} = sin\,\theta\, d\varphi\, d\theta \tag{20}$$

Moreover, the integral over $\boldsymbol{p}$ which is weighted by the orientation distribution function $\psi(\theta,\varphi)$ is utilized to obtain the second and fourth-order orientation tensor. Moreover, the orientation tensor is always symmetric and the summation of its diagonal terms is equal to one. It should be noted that the components of the orientation tensor can be used to understand the orientation of fibers. For example, ($a_{11}=1,\ a_{22}=0,\ a_{33}=0$) is a representation for completely aligned fibers and ($a_{11}=1/3,\ a_{22}=1/3,\ a_{33}=1/3$) represents three-dimensional random fibers.

The main idea of the two-step homogenization approach is to decompose the composite microstructures into several groups (pseudo-grains) and obtain the effective behavior of the whole misaligned structure based on the stiffness of all grains. This strategy is also widely used for the nonlinear mechanical behavior of composites. Fig. 3 schematically

demonstrates the use of Pseudo-grain discretization in the two-step homogenization approach for SFRPs. First, it is needed to decompose the microstructure into several grains with perfectly aligned fibers where each grain includes fibers with the same orientation and aspect ratio. Then, the first step of homogenization (previous subsection) is conducted to obtain the effective elastic behavior of aligned fibers in each grain. It should be highlighted that in this stage the mean-field homogenization or finite element modeling (MT/FE) can be performed to predict the homogenized response of aligned SFRPs where the 3D orientation transformation can be used to modify the stiffness tensors based on the orientation of fibers. After having the homogenized behavior of each grain, the stiffness averaging approaches can be adopted to estimate the homogenized response of the SFRP with misaligned fibers.

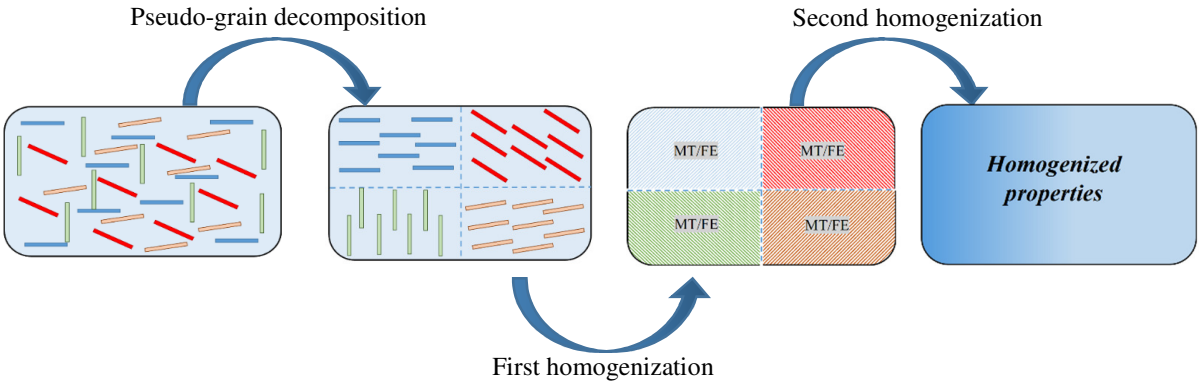

Figure 3. Schematic description of two-step homogenization method using Pseudo-grain approach.

In this research, the Voigt approach is utilized to estimate the effective response of fiber misalignment in the second step of homogenization. Recently, it was demonstrated by different researchers that this strategy leads to a reasonable approximation for the elastic response of SFRPs [20, 38].

$$\overline{\boldsymbol{C}} = \sum_{i=1}^{n} w_i < \overline{\boldsymbol{C}}_i > \ , \tag{21}$$

where w_i is the weight of each grain and $< \overline{\boldsymbol{C}}_i >$ is the rotated stiffness tensor of aligned SFRPs in the 3D dimensions. On the other hand, a complete fiber orientation distribution is not always accessible for misaligned short fibers and only the second-order orientation tensor can be provided due to the computational complexities. To resolve this issue, the fourth-order orientation tensor must be approximated using some closure approaches such as hybrid, orthotropic, natural and weighted methods [53, 55-57]. In the current work, the improved fitted orthotropic closure approach which was proposed by Chung and Kwon [58] is selected to estimate the effective elastic response of SFRPs with misaligned fibers. This approach relies on the eigenvalues of the second-order orientation tensor ($\widehat{\boldsymbol{a}}$) and only requires three independent parameters from the principal fourth-order orientation tensor ($\widehat{\boldsymbol{A}}$) that can be evaluated using the fitted constants of polynomial expansions as follows [58]

$$\begin{Bmatrix} \hat{A}_{11} \\ \hat{A}_{22} \\ \hat{A}_{33} \end{Bmatrix} = \begin{bmatrix} 0.070055 & 0.339376 & 0.590331 & -0.396796 & 0.333693 & 0.411944 \\ 0.115177 & -0.368267 & 0.252880 & 0.094820 & 0.800181 & 0.535224 \\ 1.249811 & -2.148297 & 0.898521 & -2.290157 & 1.044147 & 1.934914 \end{bmatrix} \begin{Bmatrix} 1 \\ \hat{a}_{11} \\ \hat{a}_{11}^2 \\ \hat{a}_{22} \\ \hat{a}_{22}^2 \\ \hat{a}_{11}\hat{a}_{22} \end{Bmatrix}, \tag{22}$$

where the eigenvalues of the second-order orientation tensor should satisfy the ($\hat{a}_{11} \geq \hat{a}_{22} \geq \hat{a}_{33}$) condition. It should be noted that these constants were determined using a least-square fitting of numerical solutions for the probability distribution function in various sets of flow fields. The remaining terms of the fourth-order orientation tensor (three components) in the principal directions can be obtained using the normalization conditions and the calculated orientation tensor. Further details can be found in [58].

Finally, a tensorial formulation which was proposed by Advani and Tucker [54] is used to extract the stiffness tensor of composite materials with misaligned/rotated fibers using the elastic response of composite with aligned fibers and the second and fourth-order orientation tensors (Eq. 18 and 19).

$$\left\langle \overline{C_{ijkl}} \right\rangle = B_1(a_{ijkl}) + B_2(a_{ij}\delta_{kl} + a_{kl}\delta_{ij}) + B_3(a_{ik}\delta_{jl} + a_{il}\delta_{jk} + a_{jl}\delta_{ik} + a_{jk}\delta_{il}) + B_4(\delta_{ik}\delta_{jl}) + B_5(\delta_{ik}\delta_{jl} + \delta_{il}\delta_{jk}), \tag{23}$$

where the constants $B_j = 1, 2, 3, 4, 5$ can be determined using the components of the stiffness tensor of the composite material with aligned fibers as

$$\begin{aligned} B_1 &= \overline{C}_{1111}^{\text{Aligned}} + \overline{C}_{2222}^{\text{Aligned}} - 2\overline{C}_{1122}^{\text{Aligned}} - 4\overline{C}_{1212}^{\text{Aligned}}, \\ B_2 &= \overline{C}_{1122}^{\text{Aligned}} - \overline{C}_{2233}^{\text{Aligned}}, \\ B_3 &= \overline{C}_{1212}^{\text{Aligned}} + 0.5(\overline{C}_{2233}^{\text{Aligned}} - \overline{C}_{2222}^{\text{Aligned}}), \\ B_4 &= \overline{C}_{2233}^{\text{Aligned}}, \\ B_5 &= 0.5(\overline{C}_{2222}^{\text{Aligned}} - \overline{C}_{2233}^{\text{Aligned}}). \end{aligned} \tag{24}$$

2.3. Macro-mechanical analysis

2.3.1. Enhanced laminate theory

In this study, in order to calculate the elastic response of composite materials at the macroscopic level, the enhanced classical laminated plate theory (ECLPT) [59] is adopted. The key aspect regarding the use of the enhanced laminate theory is the possibility of considering three-dimensional solutions for evaluating the triaxial and flexural response of composite materials where uniform normal stresses with zero shear tractions are considered for the upper and lower surfaces. This solution is applicable for both symmetric and non-symmetric multi-layered composites with *N* plies where each ply may have different mechanical properties. In the enhanced laminate theory the interface between the adjacent layers is considered to be perfectly bonded and the continuity of both stress and displacement fields are satisfied at the interface between the plies. Fig. 4 demonstrates the schematic description of the equivalent laminate in the enhanced laminate theory. The (X, Y and Z) represent the directions in the global coordinate system when there are fibers in more

than one orientation. As it can be seen in Fig.4, the thickness of the laminate is denoted by $2h$ and Z_i represents the height of i^{th} ply with respect to the laminate mid-plane.

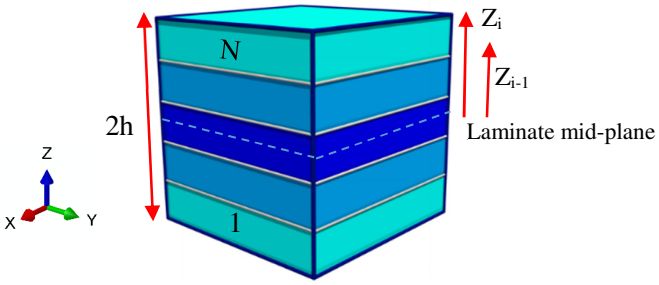

Figure 4. Demonstration of equivalent laminate in the enhanced laminate theory.

Considering the additional effects of out-of-plane normal strain in the classical laminate theory leads to the modified stiffness tensor $\tilde{C}$ of each ply, which can be determined using the following formula [59]

$$\tilde{\bar{C}}^{i}=\begin{bmatrix} \bar{C}^{i}_{11}-\frac{(\bar{C}^{i}_{13})^2}{\bar{C}^{i}_{33}} & \bar{C}^{i}_{12}-\frac{\bar{C}^{i}_{13}\bar{C}^{i}_{23}}{\bar{C}^{i}_{33}} & \frac{\bar{C}^{i}_{13}}{\bar{C}^{i}_{33}} & \bar{C}^{i}_{16}-\frac{\bar{C}^{i}_{13}\bar{C}^{i}_{36}}{\bar{C}^{i}_{33}} \\ \bar{C}^{i}_{12}-\frac{\bar{C}^{i}_{13}\bar{C}^{i}_{23}}{\bar{C}^{i}_{33}} & \bar{C}^{i}_{22}-\frac{(\bar{C}^{i}_{23})^2}{\bar{C}^{i}_{33}} & \frac{\bar{C}^{i}_{23}}{\bar{C}^{i}_{33}} & \bar{C}^{i}_{26}-\frac{\bar{C}^{i}_{23}\bar{C}^{i}_{36}}{\bar{C}^{i}_{33}} \\ \frac{\bar{C}^{i}_{13}}{\bar{C}^{i}_{33}} & \frac{\bar{C}^{i}_{23}}{\bar{C}^{i}_{33}} & \frac{1}{\bar{C}^{i}_{33}} & \frac{\bar{C}^{i}_{36}}{\bar{C}^{i}_{33}} \\ \bar{C}^{i}_{16}-\frac{\bar{C}^{i}_{13}\bar{C}^{i}_{36}}{\bar{C}^{i}_{33}} & \bar{C}^{i}_{26}-\frac{\bar{C}^{i}_{23}\bar{C}^{i}_{36}}{\bar{C}^{i}_{33}} & \frac{\bar{C}^{i}_{36}}{\bar{C}^{i}_{33}} & \bar{C}^{i}_{66}-\frac{(\bar{C}^{i}_{36})^2}{\bar{C}^{i}_{33}} \end{bmatrix}, \tag{25}$$

where $\bar{C}^{i}$ indicates the homogenized behavior of the i^{th} ply with the effect of fiber misalignment. Using the modified stiffness tensor $\tilde{C}$ of each ply, the $[A'][B'][D']$ matrices can be calculated.

$$\begin{aligned} \boldsymbol{A}^{'} &= \frac{1}{2h}\sum_{i=1}^{N}(z_i - z_{i-1})\tilde{C}^{i}_{kl}, \\ \boldsymbol{B}^{'} &= \frac{1}{2h}\sum_{i=1}^{N}\left(\frac{z_i^2 - z_{i-1}^2}{2}\right)\tilde{C}^{i}_{kl}, \\ \boldsymbol{D}^{'} &= \frac{1}{2h}\sum_{i=1}^{N}\left(\frac{z_i^3 - z_{i-1}^3}{3}\right)\tilde{C}^{i}_{kl}, \end{aligned} \tag{26}$$

Similarly, the components of the ABD stiffness matrix which include the triaxial stiffness matrix [$\boldsymbol{A}$], coupling matrix [$\boldsymbol{B}$] and bending stiffness matrix [$\boldsymbol{D}$] can be determined as follows

$$\boldsymbol{A}=\begin{bmatrix} A^{'}_{11}+\frac{(A^{'}_{13})^2}{A^{'}_{33}} & A^{'}_{12}+\frac{A^{'}_{13}A^{'}_{23}}{A^{'}_{33}} & \frac{A^{'}_{13}}{A^{'}_{33}} & A^{'}_{16}-\frac{A^{'}_{13}A^{'}_{36}}{A^{'}_{33}} \\ A^{'}_{12}+\frac{A^{'}_{13}A^{'}_{23}}{A^{'}_{33}} & A^{'}_{22}+\frac{(A^{'}_{23})^2}{A^{'}_{33}} & \frac{A^{'}_{23}}{A^{'}_{33}} & A^{'}_{26}-\frac{A^{'}_{23}A^{'}_{36}}{A^{'}_{33}} \\ \frac{A^{'}_{13}}{A^{'}_{33}} & \frac{A^{'}_{23}}{A^{'}_{33}} & \frac{1}{A^{'}_{33}} & -\frac{A^{'}_{36}}{A^{'}_{33}} \\ A^{'}_{16}-\frac{A^{'}_{13}A^{'}_{36}}{A^{'}_{33}} & A^{'}_{26}-\frac{A^{'}_{23}A^{'}_{36}}{A^{'}_{33}} & -\frac{A^{'}_{36}}{A^{'}_{33}} & A^{'}_{66}+\frac{(A^{'}_{36})^2}{A^{'}_{33}} \end{bmatrix}, \quad \boldsymbol{B}=\begin{bmatrix} B^{'}_{11}+\frac{B^{'}_{13}A^{'}_{13}}{A^{'}_{33}} & B^{'}_{12}+\frac{B^{'}_{23}A^{'}_{13}}{A^{'}_{33}} & B^{'}_{16}-\frac{B^{'}_{36}A^{'}_{13}}{A^{'}_{33}} \\ B^{'}_{12}+\frac{B^{'}_{13}A^{'}_{23}}{A^{'}_{33}} & B^{'}_{22}+\frac{B^{'}_{23}A^{'}_{23}}{A^{'}_{33}} & B^{'}_{26}-\frac{B^{'}_{36}A^{'}_{23}}{A^{'}_{33}} \\ \frac{B^{'}_{13}}{A^{'}_{33}} & \frac{B^{'}_{23}}{A^{'}_{33}} & -\frac{B^{'}_{36}}{A^{'}_{33}} \\ B^{'}_{16}-\frac{B^{'}_{13}A^{'}_{36}}{A^{'}_{33}} & B^{'}_{26}-\frac{B^{'}_{23}A^{'}_{36}}{A^{'}_{33}} & B^{'}_{66}+\frac{B^{'}_{36}A^{'}_{36}}{A^{'}_{33}} \end{bmatrix}, \quad \boldsymbol{D}=\begin{bmatrix} D^{'}_{11}+\frac{B^{'}_{13}B^{'}_{13}}{A^{'}_{33}} & D^{'}_{12}+\frac{B^{'}_{23}B^{'}_{13}}{A^{'}_{33}} & D^{'}_{16}-\frac{B^{'}_{36}B^{'}_{13}}{A^{'}_{33}} \\ D^{'}_{12}+\frac{B^{'}_{13}B^{'}_{23}}{A^{'}_{33}} & D^{'}_{22}+\frac{B^{'}_{23}B^{'}_{23}}{A^{'}_{33}} & D^{'}_{26}-\frac{B^{'}_{36}B^{'}_{23}}{A^{'}_{33}} \\ \frac{B^{'}_{13}}{A^{'}_{33}} & \frac{B^{'}_{23}}{A^{'}_{33}} & -\frac{B^{'}_{36}}{A^{'}_{33}} \\ D^{'}_{16}-\frac{B^{'}_{13}B^{'}_{36}}{A^{'}_{33}} & D^{'}_{26}-\frac{B^{'}_{23}B^{'}_{36}}{A^{'}_{33}} & D^{'}_{66}+\frac{B^{'}_{36}B^{'}_{36}}{A^{'}_{33}} \end{bmatrix},$$

$$\boldsymbol{D}=\begin{bmatrix} D_{11}^{'}+\frac{(B_{13}^{'})^2}{A_{33}^{'}} & D_{12}^{'}+\frac{B_{13}^{'}B_{23}^{'}}{A_{33}^{'}} & D_{16}^{'}-\frac{B_{13}^{'}B_{36}^{'}}{A_{33}^{'}} \\ D_{12}^{'}+\frac{B_{13}^{'}B_{23}^{'}}{A_{33}^{'}} & D_{22}^{'}+\frac{(B_{23}^{'})^2}{A_{33}^{'}} & D_{26}^{'}-\frac{B_{23}^{'}B_{36}^{'}}{A_{33}^{'}} \\ D_{16}^{'}-\frac{B_{13}^{'}B_{36}^{'}}{A_{33}^{'}} & D_{26}^{'}-\frac{B_{23}^{'}B_{36}^{'}}{A_{33}^{'}} & D_{66}^{'}+\frac{(B_{36}^{'})^2}{A_{33}^{'}} \end{bmatrix}. \tag{27}$$

For more information about the derivation of the aforementioned formulas, the reader can refer to [59]. Therefore, the linear relation between the effective stress/moment and strain/curvature in the global coordinate system (X, Y, Z) can be defined as

$$\begin{Bmatrix} \sigma_{xx} \\ \sigma_{yy} \\ \sigma_{zz} \\ \tau_{xy} \\ M_{xx} \\ M_{yy} \\ M_{xy} \end{Bmatrix}=\begin{bmatrix} [\boldsymbol{A}]_{4\times4} & [\boldsymbol{B}]_{4\times3} \\ [\boldsymbol{B}]^{T}_{3\times4} & [\boldsymbol{D}]_{3\times3} \end{bmatrix}\begin{Bmatrix} \varepsilon_{xx} \\ \varepsilon_{yy} \\ \varepsilon_{zz} \\ \gamma_{xy} \\ \hat{\varepsilon}_{xx} \\ \hat{\varepsilon}_{yy} \\ \hat{\varepsilon}_{xy} \end{Bmatrix}, \tag{28}$$

where $\boldsymbol{\varepsilon}$ and $\hat{\boldsymbol{\varepsilon}}$ refer to the strain and curvature components, respectively. By inverting the above equation, it is also possible to extract the engineering constants for the multi-layered model as

$$\begin{Bmatrix} \varepsilon_{xx} \\ \varepsilon_{yy} \\ \varepsilon_{zz} \\ \gamma_{xy} \\ \hat{\varepsilon}_{xx} \\ \hat{\varepsilon}_{yy} \\ \hat{\varepsilon}_{xy} \end{Bmatrix}=\begin{bmatrix} \frac{1}{E_{xx}} & -\frac{\upsilon_{xy}}{E_{xx}} & -\frac{\upsilon_{xz}}{E_{xx}} & -\frac{\lambda_{xy}}{E_{xx}} & -\frac{\hat{\upsilon}_{xy}}{\hat{E}_{xx}} & -\frac{\hat{\eta}_{xy}}{\hat{E}_{yy}} & -\frac{\hat{\lambda}_{xy}}{\hat{E}_{xx}} \\ -\frac{\upsilon_{xy}}{E_{xx}} & \frac{1}{E_{yy}} & -\frac{\upsilon_{yz}}{E_{yy}} & -\frac{\lambda_{xz}}{E_{yy}} & -\frac{\hat{\upsilon}_{xz}}{\hat{E}_{xx}} & -\frac{\hat{\eta}_{xz}}{\hat{E}_{yy}} & -\frac{\hat{\lambda}_{xz}}{\hat{E}_{xx}} \\ -\frac{\upsilon_{xy}}{E_{xx}} & -\frac{\upsilon_{yz}}{E_{yy}} & \frac{1}{E_{zz}} & -\frac{\lambda_{yz}}{E_{xx}} & -\frac{\hat{\upsilon}_{yz}}{\hat{E}_{xx}} & -\frac{\hat{\eta}_{yz}}{\hat{E}_{yy}} & -\frac{\hat{\lambda}_{yz}}{\hat{E}_{xx}} \\ -\frac{\lambda_{xy}}{E_{xx}} & -\frac{\lambda_{xz}}{E_{xx}} & -\frac{\lambda_{yz}}{E_{xx}} & \frac{1}{G_{xy}} & -\frac{\hat{\upsilon}_{S}}{\hat{E}_{xx}} & -\frac{\hat{\eta}_{S}}{\hat{E}_{yy}} & -\frac{\hat{\lambda}_{S}}{\hat{E}_{xx}} \\ -\frac{\hat{\upsilon}_{xy}}{\hat{E}_{xx}} & -\frac{\hat{\upsilon}_{xz}}{\hat{E}_{xx}} & -\frac{\hat{\upsilon}_{yz}}{\hat{E}_{xx}} & -\frac{\hat{\upsilon}_{S}}{\hat{E}_{xx}} & \frac{1}{\hat{E}_{xx}} & -\frac{\hat{\delta}_{xy}}{\hat{E}_{xx}} & -\frac{\hat{\beta}_{xy}}{\hat{E}_{xx}} \\ -\frac{\hat{\eta}_{xy}}{\hat{E}_{yy}} & -\frac{\hat{\eta}_{xz}}{\hat{E}_{yy}} & -\frac{\hat{\eta}_{yz}}{\hat{E}_{yy}} & -\frac{\hat{\eta}_{S}}{\hat{E}_{yy}} & -\frac{\hat{\delta}_{xy}}{\hat{E}_{xx}} & \frac{1}{\hat{E}_{yy}} & -\frac{\hat{\beta}_{xz}}{\hat{E}_{xx}} \\ -\frac{\hat{\lambda}_{xy}}{\hat{E}_{xx}} & -\frac{\hat{\lambda}_{xz}}{\hat{E}_{xx}} & -\frac{\hat{\lambda}_{yz}}{\hat{E}_{xx}} & -\frac{\hat{\lambda}_{S}}{\hat{E}_{xx}} & -\frac{\hat{\beta}_{xy}}{\hat{E}_{xx}} & -\frac{\hat{\beta}_{xz}}{\hat{E}_{xx}} & \frac{1}{\hat{G}_{xy}} \end{bmatrix}^{-1}\begin{Bmatrix} \sigma_{xx} \\ \sigma_{yy} \\ \sigma_{zz} \\ \tau_{xy} \\ M_{xx} \\ M_{yy} \\ M_{xy} \end{Bmatrix}, \tag{29}$$

where λ, η and β show, respectively, the effects of shear stress and moments, coupling counterpart of Poisson's ratio, and flexural counterpart of Poisson's ratio. Note that the superscript (^) refers to the flexural components of the model.

2.3.2. Second-order homogenization approach

As an alternative to the enhanced laminate theory, FE modeling with second-order homogenization formulation can be used to predict both the triaxial and flexural effective properties of SFRPs by explicit modeling of all microstructural details through the thickness. The second-order homogenization technique is an efficient numerical tool for reducing the computational cost and imposing the in-plane and flexural loading conditions to RVEs/Unit cells in various length scales. Various researchers have employed this strategy for continuous fiber composite laminates as well as woven composite materials with formulations based on the 2D classical laminate theory [60-64]. According to this approach, only the in-plane periodic boundary conditions should be applied for the micro/mesostructures and the periodicity in the z-direction needs to be relaxed. Similar to the 3D PBCs, the in-plane PBCs have been imposed to correlate the

displacement fields for pairs of nodes in parallel surfaces (*x* and *y* directions). Considering the kinematics of thin plates, the displacement field corresponding to such PBCs can be described as

$$\vec{u}_\alpha^+ - \vec{u}_\alpha^- = (\boldsymbol{\varepsilon} + z\hat{\boldsymbol{\varepsilon}})(\vec{x}_\alpha^+ - \vec{x}_\alpha^-) \ , \tag{30}$$

$$u_z^+ - u_z^- = -\frac{1}{2}\hat{\boldsymbol{\varepsilon}}(\vec{x}_\alpha^+ \vec{x}_\alpha^+ - \vec{x}_\alpha^- \vec{x}_\alpha^-) \ , \tag{31}$$

where $\boldsymbol{\varepsilon}$ and $\hat{\boldsymbol{\varepsilon}}$ represent the strain and curvature tensors, respectively. Additionally, the in-plane nodal displacements at X and Y boundaries are indicated by $\vec{u}_\alpha$ while the out-of-plane (Z) nodal displacement is demonstrated by u_z. The superscripts (+ and -) denote the opposing surfaces at the boundaries. In the Abaqus software, the aforementioned constraints can be introduced using *EQUATION command. After meshing and defining the constraints for the nodes in the boundaries, seven loading conditions involving triaxial and bending components are imposed on the model to extract all the ABD matrix components based on the enhanced laminate theory. The applied loads (seven load cases) include three strains in (X, Y and XY)-directions, one uniform stress σ_{zz} to the upper and lower surfaces in the Z-direction, as well as three bending curvatures in (X, Y and XY)-directions. It should be also noted that in the existing works, only six loading conditions have been applied to obtain the ABD tensor based on the 2D classical laminate theory ignoring the effects of out-of-plane normal deformations which are important even under in-plane loading conditions especially when fibers are oriented in the out-of-plane direction.

In summary, after calculating the elastic response of composite material using MFH or FEM based on the microscopic details, the obtained results can be linked to the Pseudo-grain or Closure approaches to consider the effects of fiber misalignment in the mechanical response. Using laminate analogy for different SFRPs and hybrid composites, the effective elastic response of such materials can be coupled with the enhanced laminate theory to extract the triaxial and flexural response of the materials. In this case, it is possible to incorporate variations in the volume fraction and orientation tensor through the thickness. On the other hand, from the numerical point of view, the second-order homogenization approach can be used in finite element modeling to illustrate the validity of the suggested strategy in different length scales.

3. Results and discussion

3.1. Numerical validations

First, in order to obtain the effective elastic response of SFRPs with aligned fibers and thoroughly validate the different modeling ingredients, microscale analysis is performed using the Mori-Tanaka approach and validating with finite element modeling. For this purpose, the glass/PA6 composite (Table 1 (set #1)) is selected as a representative material for the microstructure of SFRPs while the fiber aspect ratio of Ar=20, which is a typical aspect ratio for such composite materials, is considered for the cylindrical inclusions.

Table 1: Utilized material properties for short fiber reinforced polymers.

Set	Material	E [MPa]	υ [-]	Reference
#1	*Glass fiber*	72000	0.22	[40]
	PA6	2820	0.33	
#2	*Glass fiber*	70000	0.2	[65]
	PA6	2800	0.4	[65]

The length and diameter of fibers are selected, respectively, as $l_f = 200\mu m$ and $d_f = 10\mu m$ which correspond to the aspect ratio of $Ar = 20$. For the RVEs with aligned fibers, the length of the RVEs is considered to satisfy the minimum RVE size as ($l_x \geq 2l_f$) and ($l_y = l_z \geq 5d_f$) [65]. It is clear that the RVE size depends on the volume fraction for a fixed number of fibers. To have consistency when constructing RVEs with different volume fractions, we have considered the same number of fibers (30 fibers) for all RVEs with unidirectional fibers and different volume fractions. Fig. 5 demonstrates the selected RVEs and the quality of the mesh utilized for SFRPs having 30 aligned fibers with volume fraction in the range of 0.10-0.30. The number of fibers is selected to be large enough to represent the mechanical response of SFRPs and increasing the number of fibers had no significant effects on the predicted mechanical behavior of SFRPs. As illustrated, the fibers are positioned randomly and aligned in the model and tetrahedral elements are utilized for meshing the RVEs. Due to the presence of high-stress zones near the tips of the fiber, a very fine mesh is chosen to ensure the convergence of the results. For such models with aligned fibers, more than 500,000 elements are utilized to ensure converged results for all loading cases.

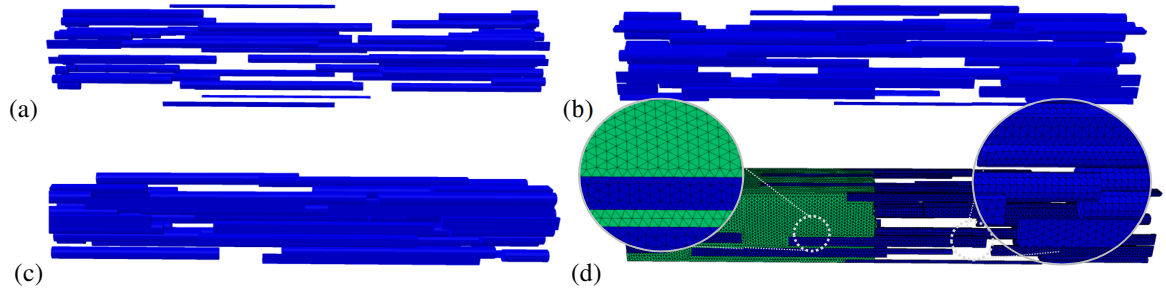

Figure 5. The utilized geometry for RVEs with 30 aligned fibers; (a) volume fraction 10%, (b) volume fraction 20%, (c) volume fraction 30% and (d) sample of mesh for RVE with volume fraction of 20%.

It should be noted that the Eshelby tensor in MFH approaches is developed for ellipsoidal shapes of the inclusion which considers a uniform strain in the inclusion for an applied eigenstrain. However, the cylindrical inclusions show variation in the internal strain and this can alter the strain concentration tensors [40]. In order to consider an equivalent ellipsoidal inclusion for the MFH based on the information of the cylindrical inclusions, two types of inclusions can be suggested; the inclusion with the same aspect ratio (Ar) and the inclusion with the same length (L) and volume (V). This strategy

was also used by different researchers (for example McCartney [66] and Rashidinejad et al. [40]) to find the equivalent ellipsoidal inclusion for cylindrical fibers.

Fig. 6 shows the prediction of the effective elastic responses of SFRPs based on the analytical and numerical approaches.

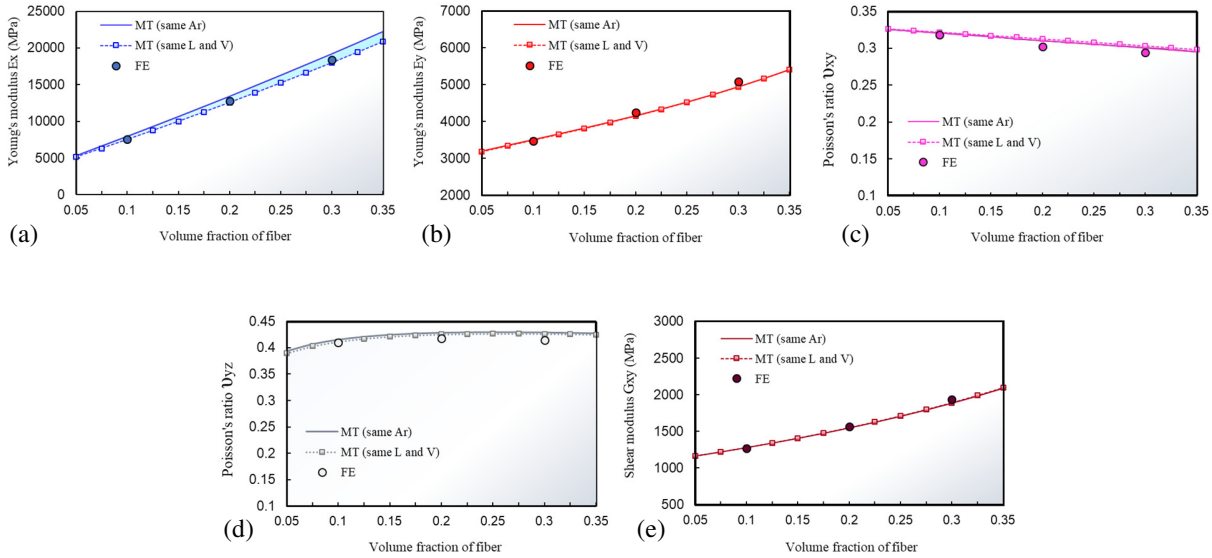

Figure 6. Obtained effective elastic constants for glass SFRPs with an aspect ratio of 20 using the Mori-Tanaka approach and finite element modeling; (a) Young's modulus E_x, (b) Young's modulus E_y, (c) Poisson's ratio υ_{xy}, (d) Poisson's ratio υ_{yz} and (e) Shear modulus G_{xy}.

Scrutinizing the obtained results demonstrates that there is a good agreement between the MT prediction and finite element data for different volume fractions. It is also clear that considering equivalent inclusions with the same length and volume (same L and V) leads to better prediction in Young's modulus in the fiber direction. It should be noted that the FE results may slightly change by modifying the number of fibers and their position. However, considering the computational expenses of the finite element modeling, the MT approach provides reasonable accuracy for the elastic behavior of aligned glass fiber reinforced polymers.

In the second step, the effects of fiber misalignment are investigated to address the possibility of extracting the effective mechanical response of SFRPs with misaligned fibers using the elastic behavior of microstructures with aligned fibers. From the numerical point of view, RVEs with misaligned fibers are generated using Digimat software [67] and linked to a commercial finite element software to provide the benchmark solutions for the two-step homogenization approaches. The microstructures have been modeled using 50 misaligned fibers with an aspect ratio of 20 and a volume fraction of 10%. The main reason for selecting a lower volume fraction is the difficulty in RVE generation for microstructures with misaligned fibers and high volume fractions using Digimat software [67]. Fig. 7 presents an illustration of the employed RVEs and their corresponding mesh. In this case, more than 750,000 tetrahedral elements have been utilized to mesh the RVEs.

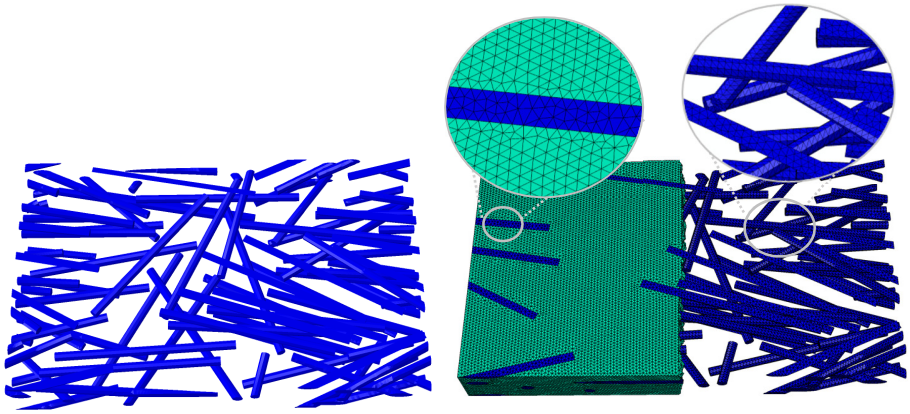

Figure 7. Utilized geometry and mesh for RVEs with 50 misaligned fibers with orientation tensor (a_{11}=0.8, a_{22}=0.2, a_{12}=0.0145).

Different homogenization strategies are conducted to capture the influence of fiber misalignment in the effective mechanical response. In the first step, the fiber orientations are directly extracted from the generated RVEs which give us exact information about the fiber orientation distributions. Considering the obtained stiffness tensors for the aligned SFRPs, the Pseudo-grain approach with Voigt orientation averaging is employed for the calculated results in both analytical and numerical methods. In the second step, it is assumed that the fiber orientation distributions are not clearly known and only the second-order orientation tensor of the generated RVEs is given. In this case, the closure approximation is utilized in order to predict the stiffness tensor for SFRPs with misaligned fibers (Eq. 23) via the estimated fourth-order orientation tensor. Fig. 8 reports the effects of fiber distribution on the mechanical response of SFRPs. It should be noted that in this analysis the a_{12} component of the second-order orientation tensor is also considered for estimating the homogenized response based on the closure approach.

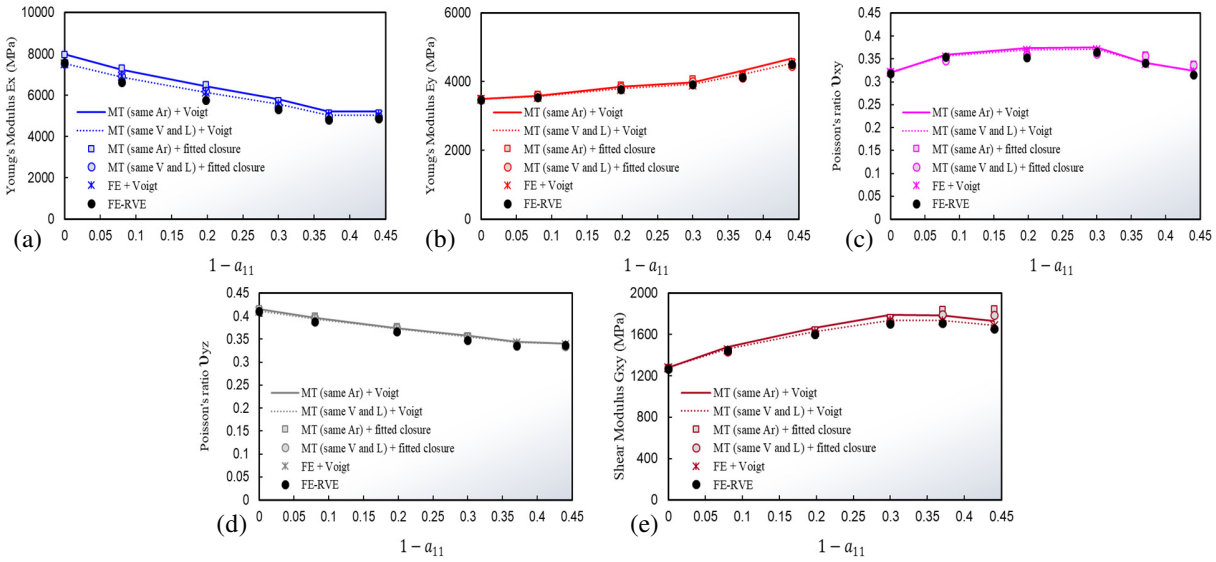

Figure 8. Obtained effective elastic constants for glass SFRPs with an aspect ratio of 20 and the volume fraction of 10% based on different orientation averaging approaches and finite element modeling; (a) Young's modulus E_x, (b) Young's modulus E_y, (c) Poisson's ratio υ_{xy}, (d) Poisson's ratio υ_{yz} and (e) Shear modulus G_{xy}.

The obtained data illustrates that there is no significant difference between the results of different approaches. However, it can be clearly seen that the accuracy in the prediction of SFRPs stiffness with aligned fibers has some effects on the prediction of the homogenized response of SFRPs with misaligned fibers. The results also show that the Voigt approach (MT with same *L* and *V*, as well as FE model) and fitted closure (MT with same *L* and *V*) approach lead to almost close predictions for the elastic constants in most of the orientation configurations. It should be noted that in the Voigt approach all the details of fiber orientation are given to predict the effects of fiber misalignment while in the closure approach only the second-order orientation tensor is provided. As expected, Voigt predictions are slightly higher than those evaluated by FE-RVE models due to imposing uniform strain conditions when using this method. This finding also supports the observation of different researchers such as Naili et al. [20] and Mirkhalaf et al. [21] where they linked the mechanical response of simplified (2D and 3D) unit cells to the orientation averaging approaches. In summary, the obtained results indicate that there are no remarkable differences between the predictions obtained from the two-step homogenization based on MT results and FE simulation of RVEs with aligned fiber for the selected typical stiffness contrasts and volume fractions of glass SFRPs.

In the third step, the mechanical response of SFRPs microstructures is linked to the enhanced laminate theory to calculate the structural level stiffness of materials. To do so, the validity of the enhanced laminate theory is first studied using the second-order homogenization method based on FE analysis. For this reason, a SFRPs laminate made of glass fiber reinforced polymer (Table 1) with complex microstructure (randomly oriented fibers) and aspect ratio of $Ar=20$ is selected. The equivalent laminate has two sets of microstructures with a thickness of $1mm$ (see Fig. 9(a)). The volume fraction in the lower and upper plies is chosen as $\vartheta_i = 0.1$ with completely aligned fibers while this value changes to $\vartheta_i = 0.2$ for the middle ply with three-dimensional randomly distributed fibers. The 3D linear closure approach [53, 54], which provides an accurate calculation for the fourth-order orientation tensor of completely randomly distributed fibers, is employed to compute the effective elastic response for 3D random microstructures. Using MT homogenization, the evaluated effective elastic properties of each ply are reported in Table 2. Then, the homogenized elastic responses have been specified as material properties of the three plies in the enhanced laminate theory and FE second-order homogenization. To accurately compute the flexural response of those materials in finite element simulations, the 20-node quadratic brick element (C3D20) is adopted for meshing the model (see Fig. 9(b)).

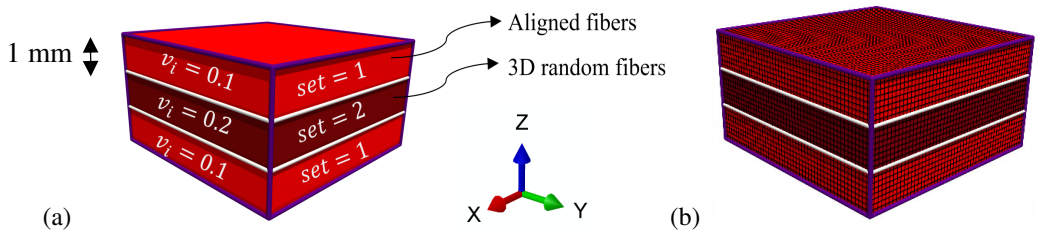

Figure 9. Selected SFRPs laminate and utilized mesh in finite element modeling.

Table 2: Homogenized elastic response of SFRPs with an aspect ratio of *Ar=20* based on MT.

set	v_i [-]	E_{xx} [MPa]	E_{yy} [MPa]	E_{zz} [MPa]	υ_{xy} [-]	υ_{xz} [-]	υ_{yz} [-]	G_{xy} [MPa]	G_{xz} [MPa]	G_{yz} [MPa]
1	0.1	7973.81	3502.24	3502.24	0.3203	0.3203	0.4156	1279.69	1279.69	1236.99
2	0.2	5547.82	5547.82	5547.82	0.2987	0.2987	0.2987	2135.92	2135.92	2135.92

The ABD matrix is then obtained based on the provided homogenized response of the laminate. According to the evaluated results for both analytical and numerical approaches, it is completely clear that the enhanced laminate theory provides exact results for all the components of the ABD matrix. It is worth mentioning that the computational cost of the FE simulation considering second-order homogenization takes more than one hour for such laminate. However, only 0.1 second is needed to run the enhanced laminate theory for such model. Fig. 10 demonstrates the S_{xx} contour of the stress fields for the selected SFRP laminate under the axial bending strain of $\hat{\varepsilon}_{xx} = 0.01$ while the other strain components are considered to be traction-free. The effective elastic properties of the SFRP laminate are provided in Table 3.

$$\boldsymbol{ABD}_{ECLPT} = \begin{bmatrix} 8737.8 & 2542.9 & 2488.1 & 0 & 0 & 0 & 0 \\ 2542.9 & 5641.6 & 2515.7 & 0 & 0 & 0 & 0 \\ 2488.1 & 2515.7 & 5426.8 & 0 & 0 & 0 & 0 \\ 0 & 0 & 0 & 1565.1 & 0 & 0 & 0 \\ 0 & 0 & 0 & 0 & 6199.7 & 898.8 & 0 \\ 0 & 0 & 0 & 0 & 898.8 & 2817.9 & 0 \\ 0 & 0 & 0 & 0 & 0 & 0 & 983.6 \end{bmatrix}, \quad \boldsymbol{ABD}_{FE} = \begin{bmatrix} 8737.8 & 2542.9 & 2488.1 & 0 & 0 & 0 & 0 \\ 2542.9 & 5641.6 & 2515.7 & 0 & 0 & 0 & 0 \\ 2488.1 & 2515.7 & 5426.8 & 0 & 0 & 0 & 0 \\ 0 & 0 & 0 & 1565.1 & 0 & 0 & 0 \\ 0 & 0 & 0 & 0 & 6199.7 & 898.8 & 0 \\ 0 & 0 & 0 & 0 & 898.8 & 2817.9 & 0 \\ 0 & 0 & 0 & 0 & 0 & 0 & 983.6 \end{bmatrix}$$

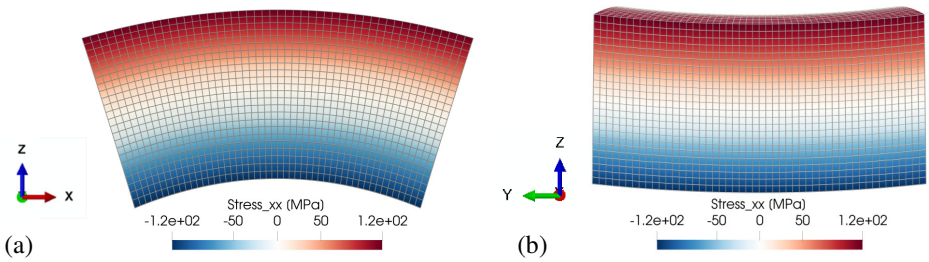

Figure 10. Stress field of SFRP laminate under $\hat{\varepsilon}_{xx} = 0.01$ bending strain; (a) x-z view, (b) y-z view.

Table 3: Predicted effective elastic constants of SFRPs laminate based on the enhanced laminate theory.

E_{xx} [MPa]	E_{yy} [MPa]	E_{zz} [MPa]	υ_{xy} [-]	υ_{xz} [-]	υ_{yz} [-]	G_{xy} [MPa]	$\hat{E}_{xx}$ [MPa×mm^2]	$\hat{E}_{yy}$ [MPa×mm^2]	$\hat{\delta}_{xy}$ [-]	$\hat{G}_{xy}$ [MPa×mm^2]
7165.66	4221.26	4063.42	0.3105	0.3145	0.3797	1565.10	5913.04	2687.61	0.3190	983.56

After checking the validity of the enhanced laminate theory for SFRPs with complex microstructure, this strategy has been employed for hybrid composite microstructures. In this regard, a hybrid composite laminate made of continuous fiber laminae and SFRPs with a stacking sequence of [UD, SFRP, UD] is selected. The thickness of each ply is chosen as t=0.1 mm, where the directions of fibers in the continuous fiber lamina and SFRPs are specified as 0° and 90°, respectively. The main reason for selecting rather thin ply thicknesses is the very high computational cost of the FE modeling in the microscale level. Also, the volume fractions of the continuous fiber plies and the SFRP ply are defined

as 60% and 13%, respectively. Due to the high volume fraction of the continuous fiber lamina, both MT and finite element RVE are utilized to compute the elastic properties of these unidirectional plies. A 3D RVE with random packing of continuous fibers is generated for the continuous fiber composite and 20-node quadratic brick elements are utilized to mesh the model (see Fig. 11 (a)). Table 4 presents the evaluated homogenized response of the continuous fiber composite lamina using the analytical and numerical approaches. As it was expected, due to the high volume fraction of fibers, a higher difference between the MT approach and FE modeling is observed.

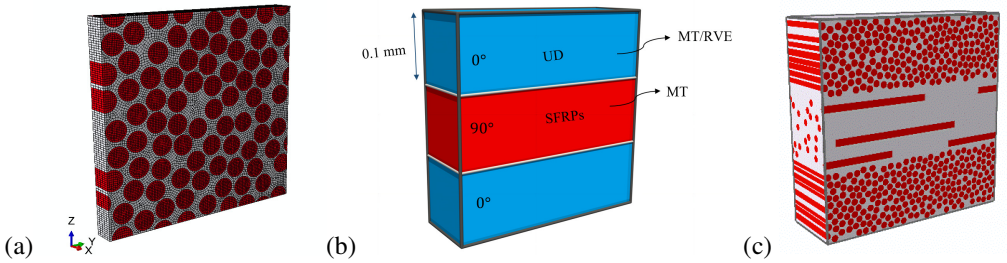

(a) (b) (c)

Figure 11. Selected material for evaluating the mechanical behavior of continuous fiber lamina/SFRPs hybrid laminate;

. (a) Continuous fiber RVE, (b) Homogenized hybrid laminate, (c) FE-Laminate RVE at the microscopic level.

Table 4: Homogenized elastic response of continuous fiber lamina with volume fraction of 60% based on MT and FE-RVE.

Method	v_i [-]	E_{xx} [MPa]	E_{yy} [MPa]	E_{zz} [MPa]	υ_{xy} [-]	υ_{xz} [-]	υ_{yz} [-]	G_{xy} [MPa]	G_{xz} [MPa]	G_{yz} [MPa]
MT	0.6	44338.1	9249.6	9249.6	0.2570	0.2570	0.4149	3741.1	3741.1	3268.7
FE-UD-RVE	0.6	44365.1	10884.9	10723.0	0.2542	0.2551	0.3544	4189.1	4100.2	3923.1

The obtained homogenized response of materials has been specified in the hybrid mesoscale laminate to be utilized in the enhanced laminate theory for computing the elastic response (see Fig. 11 (b)). For the SFRPs with an aspect of 20, only the MT approach is used to calculate the elastic response considering the same length (L) and volume (V) for the inclusion. Finally, a microstructural laminate with the same material is generated to show the performance and validity of the proposed strategy for complex structures. Fig. 11 (c) shows the defined FE-Laminate at the microscale level. The results of the different homogenization approaches are summarized in Table 5. The comparison between the results of the different approaches reveals that there is a good agreement between the ECLPT approach with FE-MT homogenized response and the microstructural analysis of the hybrid laminate (FE-Laminate). Moreover, the ECLPT with MT-MT is also able to predict the mechanical response with an encouraging small run-time on a Core i7 Central Processing Unit (CPU) with 32 Gigabytes Random Access Memory (RAM) in a 64-bit operating system. However, the error increases due to having a high volume fraction in the continuous fiber plies and this case cannot be very well predicted by the MT approach.

Table 5: Predicted effective elastic constants of hybrid laminate based on FE-Laminate modeling and enhanced laminate theory.

Model	E_{xx} [MPa]	E_{yy} [MPa]	E_{zz} [MPa]	υ_{xy} [-]	υ_{xz} [-]	υ_{yz} [-]	G_{xy} [MPa]	$\hat{E}_{xx}$ [MPa×mm^2]	$\hat{E}_{yy}$ [MPa×mm^2]	$\hat{\delta}_{xy}$ [-]	$\hat{G}_{xy}$ [MPa×mm^2]	Run time
ECLPT, (MT-MT)	30819.12	9253.18	6715.61	0.2147	0.3097	0.4207	2945.90	321.27	69.38	0.2523	27.40	0.1 sec
ECLPT, (FE-MT)	30837.18	10338.01	7226.52	0.2173	0.3050	0.3793	3244.58	321.47	81.19	0.2503	30.63	15 min
FE-Laminate	30656.67	10632.97	7183.91	0.2133	0.3064	0.3831	3327.58	317.56	81.22	0.2500	31.10	36 hours

In addition, the importance of the proposed strategy for obtaining the elastic response of such materials is further investigated by comparing the individual components of the ABD matrix obtained from the developed methodology and the Voigt approach. The Voigt approach is a widely used methodology for estimating the stiffness tensor of laminated structures in addition to the orientation averaging. This approach relies on the summation of the stiffness tensor considering uniform strain in all directions (equation (21)) ignoring the interaction between in-plane and out-of-plane deformations. The corresponding results for the assumed hybrid laminate obtained from the enhanced laminate theory, FE modeling and Voigt approach are indicated in equation (32). It can be clearly seen that the use of the Voigt assumption might lead to considerable errors in estimating the components of the stiffness tensor when comparing to the FE (MT-MT) approach. For the assumed geometry, the errors are in the range (0.33%-16.68%) for the different stiffness components where the maximum errors are related to the out-of-plane components of the stiffness tensor. It can be seen that assuming uniform strains for all loading directions (Voigt approach) will affect the in-plane components of the stiffness tensor as well, including the interaction between the in-plane and out-of-plane properties. The variation in the out-of-plane properties normally happens in SFRPs due to the orientation distribution of fibers (possibly oriented in 3D directions), volume fraction fluctuation, material properties or localized damages.

$$\boldsymbol{ABD}_{\boldsymbol{ECLPT(MT-MT)}}=\begin{bmatrix} 32572.1 & 3470.8 & 3257.8 & 0 & 0 & 0 & 0 \\ 3470.8 & 10987.0 & 3589.1 & 0 & 0 & 0 & 0 \\ 3257.8 & 3589.1 & 8031.4 & 0 & 0 & 0 & 0 \\ 0 & 0 & 0 & 2945.9 & 0 & 0 & 0 \\ 0 & 0 & 0 & 0 & 325.7 & 17.8 & 0 \\ 0 & 0 & 0 & 0 & 17.8 & 70.3 & 0 \\ 0 & 0 & 0 & 0 & 0 & 0 & 27.4 \end{bmatrix}, \boldsymbol{ABD}_{\boldsymbol{FE(MT-MT)}}=\begin{bmatrix} 32572.1 & 3470.8 & 3257.8 & 0 & 0 & 0 & 0 \\ 3470.8 & 10987.0 & 3589.1 & 0 & 0 & 0 & 0 \\ 3257.8 & 3589.1 & 8031.4 & 0 & 0 & 0 & 0 \\ 0 & 0 & 0 & 2945.9 & 0 & 0 & 0 \\ 0 & 0 & 0 & 0 & 325.7 & 17.8 & 0 \\ 0 & 0 & 0 & 0 & 17.8 & 70.3 & 0 \\ 0 & 0 & 0 & 0 & 0 & 0 & 27.4 \end{bmatrix}$$

$$\boldsymbol{C}_{\boldsymbol{VOIGT(MT-MT)}}=\begin{bmatrix} 32680.8 & 3626.1 & 3639.4 & 0.0 \\ 3626.1 & 11208.7 & 4134.0 & 0.0 \\ 3639.4 & 4134.0 & 9370.8 & 0.0 \\ 0.0 & 0.0 & 0.0 & 2945.9 \end{bmatrix}, \quad \boldsymbol{VOIGT\_Errors(\%)}=\begin{bmatrix} 0.33 & 4.47 & 11.71 & 0 \\ 4.47 & 2.02 & 15.18 & 0 \\ 11.71 & 15.18 & 16.68 & 0 \\ 0 & 0 & 0 & 0 \end{bmatrix} \tag{32}$$

Finally, in order to complete the validation of the laminate analogy approach for SFRPs with through-thickness varying microstructures, it is important to check whether the homogenization of SFRPs at different thickness coordinates and using homogenized properties for each ply can be trusted when predicting the flexural response of SFRPs. To do so, micro- and meso-scale FE simulations are utilized to obtain the triaxial and bending behavior of the SFRPs with an aspect of 20. Therefore, SFRP samples with [0, 90, 0] layers are considered. The thickness of the SFRP plies for 0° and 90° layers are, respectively, 0.12 mm and 0.06 mm. Similar to the previous case, the reason to assume these small ply

thicknesses is to reduce the computational costs of FEM modeling. Fig. 12 shows a sample of the mesh employed for the RVE with a volume fraction of 25% at the microscale level. On the other hand, the homogenized response of SFRPs is defined based on MT mean-field homogenization (with same *L* and *V*) for the meso-scale RVEs and ECLPT approaches.

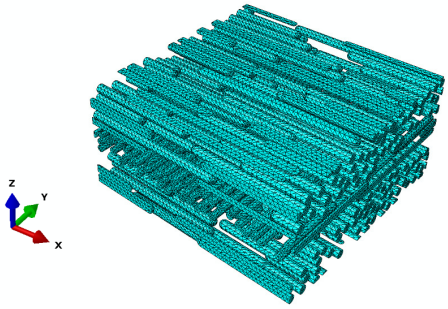

Figure 12. Sample of utilized mesh for FE modeling of multiply glass SFRPs with an aspect ratio of 20 and volume fraction 25% at the microscopic level.

Fig. 13 presents the results for the triaxial and flexural properties of SFRPs in different length scales. The comparison of the results shows a perfect agreement in the elastic constants of SFRPs based on the ECLPT and meso-scale RVEs. Additionally, the results of micro-scale RVEs are in good agreement with those of the meso-scale analysis confirming the validity of the laminate analogy for SFRPs with through-thickness varying microstructures. The run time (using the previously described computer) for the micro-scale RVEs is more than 20 hours for such simple multi-ply SFRPs while the computational cost for the MFH-ECLPT approach is less than a second.

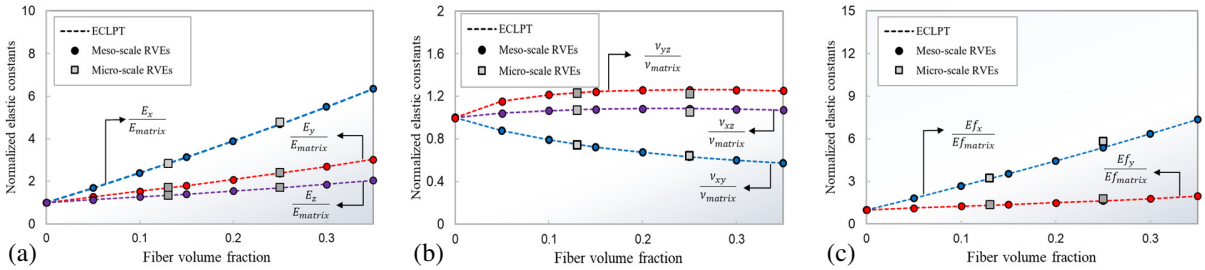

Figure 13. Elastic constants for multi-ply glass SFRPs with an aspect ratio of 20; (a) Normalized Young's modulus, (b) Normalized Poisson's ratio, and (c) Normalized flexural constant.

3.2. Experimental validation

In order to demonstrate the physical relevance and applicability of the proposed multi-scale strategy for real composite materials, the experimental investigation of short fiber reinforced polymer of Holmström et al. [39] is selected. Different tensile tests were performed in the aforementioned study for injection molded samples with high-quality digital image correlation (DIC) measurements. As discussed in the previous sections, the microstructural details of SFRPs play an important role in the mechanical behavior of such material. Therefore, it is essential to have accurate information about the fiber length, orientation and volume fraction distribution of the material. The details of orientation tensor and volume fraction through the thickness were presented based on micro-CT image analysis [39]. Fig. 14 demonstrates the variation

of the volume fraction and orientation tensor components through the thickness for glass SFRPs with the weight fraction of 30%. The average aspect ratio of the fibers was also given as $Ar = 29$ based on the manual evaluation.

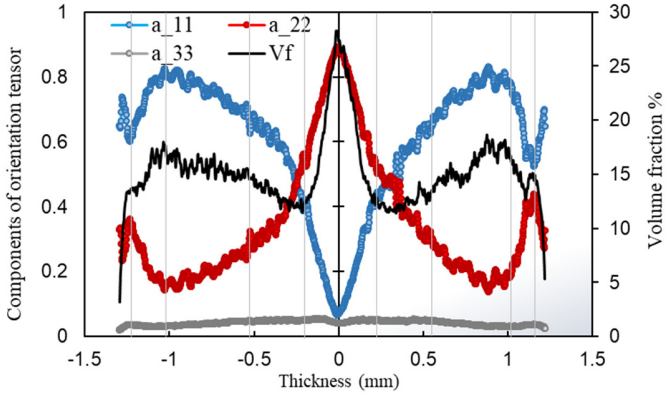

Figure 14. Components of second-order orientation tensor ***a*** (Eq. 18) and volume fraction through the thickness based on the micro-CT image information (reported in [39]).

It can be seen that there is a high variation in the components of the orientation tensor and also the volume fraction through the thickness. Therefore, the sample has been decomposed into 10 layers and linked to the suggested multiscale strategy for obtaining the elastic behavior of SFRP, where the closure approach is employed for considering the effects of fiber misalignment based on the MT stiffness tensor. Additionally, the proficiency of the suggested method is investigated using the recently published results about the elastic response of SFRPs based on the artificial neural networks (ANN) [65] and also different FE orientation averaging approaches (OA-Voigt, OA-Reuss and OA-Self-Consistent (SC)) [21]. It must be pointed out that the mentioned works [21, 65] are FE-based studies where the stiffness tensors are calculated using numerical simulations. In these works [21, 65], the average orientation tensor and average volume fraction are utilized to calculate the elastic constants instead of using the accurate through-thickness variation of microstructures. The elastic behavior of materials is defined using the material properties selected in [65] to have a consistent comparison which is given in Table 1 (set #2). Fig. 15 illustrates the comparison between the experimental measurements and different numerical and analytical strategies. It should be noted that the angle of the samples was reported clockwise based on the in-plane projection of the samples with respect to the mold flow direction (0°).

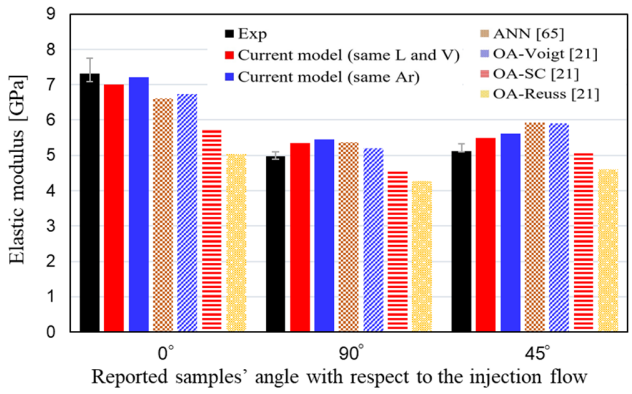

Figure 15: Obtained elastic behavior for SFRPs with 30% weight fraction using different approaches.

As it can be seen in Fig. 15, the obtained results from the suggested strategy are in good agreement with those measured by high-quality experimental tests. It should be noted that the variation of the volume fraction and orientation tensor through the thickness was easily considered in the suggested framework based on the MFH. However, it would be a time-consuming and challenging task to consider such variations in the FE-based approaches as it would be the case for the approaches in Ref [21, 65]. One might argue that the in-plane axial Young's modulus obtained from the average orientation tensor and average volume fraction [21, 65] are still in an acceptable agreement with the experimental results. Readers should take into account that the effects of through-thickness variation of the microstructures are more important for bending and out-of-plane properties. However, these parameters are much more difficult to be measured experimentally and are rarely reported in the literature. The current approach does not need time-consuming FE-based approaches for estimating stiffness tensors and at the same time incorporates the details of the microstructures in the analysis providing a fast and robust multiscale strategy for predicting all (in-plane, out-of-plane and bending) SFRPs effective properties.

It should be highlighted that the applicability of the suggested strategy is not limited to the elastic behavior of SFRPs and it can be used for different types of nonlinear behaviors of SFRPs such as damage, failure, thermo-viscoelasticity and viscoplasticity. Additionally, the suggested method has the potential assist with reverse engineering for estimating the microstructural details such as average aspect ratio, orientation tensors and core, shell layers thicknesses and elastic response of the matrix.

Conclusions

A hierarchical multi-scale strategy was proposed to predict the effective response of SFRPs having complex microstructures (variation in volume fraction and orientation distribution through the thickness) under triaxial (in-plane, out-of-plane) and flexural loading conditions. In this regard, finite element modeling and mean-field homogenization were performed to predict the effective elastic response of completely aligned Glass/Polyamide6 SFRPs. The evaluated results reveal that the MT approach can provide a good estimation for the homogenized behavior of glass SFRPs. It was also demonstrated that considering equivalent ellipsoidal inclusion with the same length and volume in the mean-field homogenization approach can provide better results for the Young's modulus in the fiber direction. Moreover, the effects of fiber misalignment on the effective elastic response of SFRPs were investigated using different approaches. It was observed that the accuracy of the prediction for the stiffness tensor of SFRPs with aligned fibers has effects on the prediction of the elastic response for microstructures with misaligned fibers. The evaluated results demonstrated that there are no remarkable differences between two-step homogenization based on FE simulation of RVEs and MT (same V and L) for the selected material. Furthermore, the effective elastic response of mean-field homogenization and FE simulation were successfully linked to a 3D enhanced laminate theory where the orientation averaging can be performed

to account for the fiber distribution effects in the homogenized response of each ply. On the other hand, the second-order homogenization approach was fully coupled with the enhanced laminate theory by adding a uniform stress loading condition to the upper and lower surface. The second-order homogenization approach was employed to analyze micro- and meso-scale SFRPs and hybrid composite systems. It was proven that the enhanced laminate theory can accurately predict the effective elastic response of materials with through-thickness varying microstructures when the homogenized response of each ply is accurately predicted. Moreover, for the homogenized behavior of microstructures, the analytical, numerical, as well as a combination of these two methods, can be used in the proposed multi-scale strategy. Finally, the efficacy of the suggested strategy is validated using high-quality experimental measurements from the literature. The current work does not attempt to predict the amount of thermal or moisture residual stresses which have important effects on the onset of non-linear behavior. A future experimental work combined with the methodology presented here is needed to estimate the level of residual stresses.

Acknowledgments

The work leading to this publication has been funded by the ICON project "ProPeL", which fits in the MacroModelMat (M3) research program, coordinated by Siemens (Siemens Digital Industries Software, Belgium), and funded by SIM (Strategic Initiative Materials in Flanders) and VLAIO (Flemish government agency Flanders Innovation & Entrepreneurship). The work of M. Hajikazemi forms part of the research programme of DPI, project 812T17. M. Hajikazemi also acknowledges the financial support of Fonds voor Wetenschappelijk Onderzoek FWO–Vlaanderen (Grant No. 1202522N).

References:

[1] K. Wang, S. Pei, Y. Li, J. Li, D. Zeng, X. Su, X. Xiao, N. Chen, In-situ 3D fracture propagation of short carbon fiber reinforced polymer composites, Composites Science and Technology 182 (2019) 107788.

[2] E. Belmonte, M. De Monte, C.-J. Hoffmann, M. Quaresimin, Damage mechanisms in a short glass fiber reinforced polyamide under fatigue loading, International Journal of Fatigue 94 (2017) 145-157.

[3] A. Bernasconi, M. Carboni, R. Ribani, On the combined use of Digital Image Correlation and Micro Computed Tomography to measure fibre orientation in short fibre reinforced polymers, Composites Science and Technology 195 (2020) 108182.

[4] M. De Monte, E. Moosbrugger, M. Quaresimin, Influence of temperature and thickness on the off-axis behaviour of short glass fibre reinforced polyamide 6.6 – Quasi-static loading, Composites Part A: Applied Science and Manufacturing 41(7) (2010) 859-871.

[5] H. Ahmadi, M. Hajikazemi, W. Van Paepegem, A computational study about the effects of ply cracking and delamination on the stiffness reduction of damaged lamina and laminate, International Journal of Damage Mechanics 0(0) 10567895211039268.

[6] S. Naderi, M. Zhang, Meso-scale modelling of static and dynamic tensile fracture of concrete accounting for real-shape aggregates, Cement and Concrete Composites 116 (2021) 103889.

[7] M. Jahanshahi, H. Ahmadi, A.R. Khoei, A hierarchical hyperelastic-based approach for multi-scale analysis of defective nano-materials, Mechanics of Materials 140 (2020) 103206.

[8] H. Kang, L. Qi, H. Dang, K. Jin, D. Thomson, H. Cui, Y. Li, Biaxial tensile failure of short carbon-fibre-reinforced PEEK composites, Composites Science and Technology 208 (2021) 108764.

[9] Y. Zhong, P. Liu, Q. Pei, V. Sorkin, A. Louis Commillus, Z. Su, T. Guo, W. Thitsartarn, T. Lin, C. He, Y.-W. Zhang, Elastic properties of injection molded short glass fiber reinforced thermoplastic composites, Composite Structures 254 (2020) 112850.

[10] L. Wang, G. Nygren, R.L. Karkkainen, Q. Yang, A multiscale approach for virtual testing of highly aligned short carbon fiber composites, Composite Structures 230 (2019) 111462.

[11] A. Isaincu, M. Dan, V. Ungureanu, L. Marșavina, Numerical investigation on the influence of fiber orientation mapping procedure to the mechanical response of short-fiber reinforced composites using Moldflow, Digimat and Ansys software, Materials Today: Proceedings 45 (2021) 4304-4309.

[12] E. Belmonte, M. De Monte, T. Riedel, M. Quaresimin, Local microstructure and stress distributions at the crack initiation site in a short fiber reinforced polyamide under fatigue loading, Polymer Testing 54 (2016) 250-259.

[13] L. Qi, W. Tian, J. Zhou, Numerical evaluation of effective elastic properties of composites reinforced by spatially randomly distributed short fibers with certain aspect ratio, Composite Structures 131 (2015) 843-851.

[14] L. Quagliato, Y. Kim, J.H. Fonseca, D. Han, S. Yun, H. Lee, N. Park, H. Lee, N. Kim, The influence of fiber orientation and geometry-induced strain concentration on the fatigue life of short carbon fibers reinforced polyamide-6, Materials & Design 190 (2020) 108569.

[15] A. Jain, S.V. Lomov, Y. Abdin, I. Verpoest, W. Van Paepegem, Pseudo-grain discretization and full Mori Tanaka formulation for random heterogeneous media: Predictive abilities for stresses in individual inclusions and the matrix, Composites Science and Technology 87 (2013) 86-93.

[16] I. Doghri, A. Ouaar, Homogenization of two-phase elasto-plastic composite materials and structures: Study of tangent operators, cyclic plasticity and numerical algorithms, International Journal of Solids and Structures 40(7) (2003) 1681-1712.

[17] I. Hanhan, R.F. Agyei, X. Xiao, M.D. Sangid, Predicting Microstructural Void Nucleation in Discontinuous Fiber Composites through Coupled in-situ X-ray Tomography Experiments and Simulations, Scientific Reports 10(1) (2020) 3564.

[18] K. Breuer, M. Stommel, RVE modelling of short fiber reinforced thermoplastics with discrete fiber orientation and fiber length distribution, SN Applied Sciences 2(1) (2019) 91.

[19] W. Tian, L. Qi, J. Zhou, J. Liang, Y. Ma, Representative volume element for composites reinforced by spatially randomly distributed discontinuous fibers and its applications, Composite Structures 131 (2015) 366-373.

[20] C. Naili, I. Doghri, T. Kanit, M.S. Sukiman, A. Aissa-Berraies, A. Imad, Short fiber reinforced composites: Unbiased full-field evaluation of various homogenization methods in elasticity, Composites Science and Technology 187 (2020) 107942.

[21] S.M. Mirkhalaf, E.H. Eggels, T.J.H. van Beurden, F. Larsson, M. Fagerström, A finite element based orientation averaging method for predicting elastic properties of short fiber reinforced composites, Composites Part B: Engineering 202 (2020) 108388.

[22] T. Mori, K. Tanaka, Average stress in matrix and average elastic energy of materials with misfitting inclusions, Acta Metallurgica 21(5) (1973) 571-574.

[23] Y. Benveniste, A new approach to the application of Mori-Tanaka's theory in composite materials, Mechanics of Materials 6(2) (1987) 147-157.

[24] O. Pierard, C. Friebel, I. Doghri, Mean-field homogenization of multi-phase thermo-elastic composites: a general framework and its validation, Composites Science and Technology 64(10) (2004) 1587-1603.

[25] Y. Wan, J. Takahashi, Tensile properties and aspect ratio simulation of transversely isotropic discontinuous carbon fiber reinforced thermoplastics, Composites Science and Technology 137 (2016) 167-176.

[26] O. Pierard, C. González, J. Segurado, J. Llorca, I. Doghri, Micromechanics of elasto-plastic materials reinforced with ellipsoidal inclusions, International Journal of Solids and Structures 44(21) (2007) 6945-6962.

[27] S. Kammoun, I. Doghri, L. Adam, G. Robert, L. Delannay, First pseudo-grain failure model for inelastic composites with misaligned short fibers, Composites Part A: Applied Science and Manufacturing 42(12) (2011) 1892-1902.

[28] L.N. McCartney, Maxwell's far-field methodology predicting elastic properties of multiphase composites reinforced with aligned transversely isotropic spheroids, Philosophical Magazine 90(31-32) (2010) 4175-4207.

[29] X. Chao, W. Tian, F. Xu, D. Shou, A fractal model of effective mechanical properties of porous composites, Composites Science and Technology 213 (2021) 108957.

[30] R. Hill, A self-consistent mechanics of composite materials, Journal of the Mechanics and Physics of Solids 13(4) (1965) 213-222.

[31] N. Laws, R. McLaughlin, The effect of fibre length on the overall moduli of composite materials, Journal of the Mechanics and Physics of Solids 27(1) (1979) 1-13.

[32] J.H. Affdl, J. Kardos, The Halpin-Tsai equations: a review, Polymer Engineering & Science 16(5) (1976) 344-352.

[33] R. Hill, The elastic behaviour of a crystalline aggregate, Proceedings of the Physical Society. Section A 65(5) (1952) 349.

[34] Z. Hashin, S. Shtrikman, A variational approach to the theory of the elastic behaviour of multiphase materials, Journal of the Mechanics and Physics of Solids 11(2) (1963) 127-140.

[35] H. Cox, The elasticity and strength of paper and other fibrous materials, British journal of applied physics 3(3) (1952) 72.

[36] C.L. Tucker Iii, E. Liang, Stiffness predictions for unidirectional short-fiber composites: Review and evaluation, Composites Science and Technology 59(5) (1999) 655-671.

[37] D. Dray, P. Gilormini, G. Régnier, Comparison of several closure approximations for evaluating the thermoelastic properties of an injection molded short-fiber composite, Composites Science and Technology 67(7) (2007) 1601-1610.

[38] A. Jain, Y. Abdin, W. Van Paepegem, S.V. Lomov, Direct Mori-Tanaka calculations of strains in ellipsoidal inclusions with multiple orientations – Comments on the papers: Naili, G. et al. Comp Sci Tech, 187: 107942, 2020 (https://doi.org/10.1016/j.compscitech.2019.107942) and Jain, A. et al., Comp Sci Tech, 87: 86–93, 2013 (https://doi.org/10.1016/j.compscitech.2013.08.009), Composites Science and Technology 190 (2020) 108068.

[39] P.H. Holmström, O.S. Hopperstad, A.H. Clausen, Anisotropic tensile behaviour of short glass-fibre reinforced polyamide-6, Composites Part C: Open Access 2 (2020) 100019.

[40] E. Rashidinejad, H. Ahmadi, M. Hajikazemi, W. Van Paepegem, Modeling of geometric configuration and fiber interactions in short fiber reinforced composites via new modified Eshelby tensors and enhanced mean-field homogenization, Mechanics of Materials (2021) 104059.

[41] S.-Y. Fu, G. Xu, Y.-W. Mai, On the elastic modulus of hybrid particle/short-fiber/polymer composites, Composites Part B: Engineering 33(4) (2002) 291-299.

[42] D.E. Sommer, S.G. Kravchenko, B.R. Denos, A.J. Favaloro, R.B. Pipes, Integrative analysis for prediction of process-induced, orientation-dependent tensile properties in a stochastic prepreg platelet molded composite, Composites Part A: Applied Science and Manufacturing 130 (2020) 105759.

[43] G. Czél, M. Jalalvand, M.R. Wisnom, Demonstration of pseudo-ductility in unidirectional hybrid composites made of discontinuous carbon/epoxy and continuous glass/epoxy plies, Composites Part A: Applied Science and Manufacturing 72 (2015) 75-84.

[44] J.C. Halpin, J.L. Karoos, Strength of discontinuous reinforced composites: I. Fiber reinforced composites, Polymer Engineering & Science 18(6) (1978) 496-504.

[45] M.M. Shokrieh, H. Moshrefzadeh-Sani, A novel laminate analogy to calculate the strength of two-dimensional randomly oriented short-fiber composites, Composites Science and Technology 147 (2017) 22-29.

[46] S.-Y. Fu, X. Hu, C.-Y. Yue, The flexural modulus of misaligned short-fiber-reinforced polymers, Composites Science and Technology 59(10) (1999) 1533-1542.

[47] T. Mura, Isotropic inclusions, Micromechanics of defects in solids, Springer Netherlands, Dordrecht, 1987, pp. 74-128.

[48] Y.P. Qiu, G.J. Weng, On the application of Mori-Tanaka's theory involving transversely isotropic spheroidal inclusions, International Journal of Engineering Science 28(11) (1990) 1121-1137.

[49] D. Garoz, F.A. Gilabert, R.D.B. Sevenois, S.W.F. Spronk, W. Van Paepegem, Consistent application of periodic boundary conditions in implicit and explicit finite element simulations of damage in composites, Composites Part B: Engineering 168 (2019) 254-266.

[50] H. Ahmadi, M. Jahanshahi, A.R. Khoei, S. Bordas, Mechanical behavior of multilayer graphene reinforced epoxy nano-composites via a hierarchical multi-scale technique, Carbon Trends 4 (2021) 100048.

[51] H. Ahmadi, M. Hajikazemi, W. Van Paepegem, Closed-form formulae for prediction of homogenized ply-properties and laminate thermo-elastic constants in symmetric laminates containing ply cracks in multiple orientations, Composite Structures 241 (2020) 112061.

[52] K. Hibbitt, Sorensen, ABAQUS/standard: User's Manual, Hibbitt, Karlsson & Sorensen1995.

[53] S.G. Advani, C.L. Tucker III, Closure approximations for three-dimensional structure tensors, Journal of Rheology 34(3) (1990) 367-386.

[54] S.G. Advani, C.L.T. III, The Use of Tensors to Describe and Predict Fiber Orientation in Short Fiber Composites, Journal of Rheology 31(8) (1987) 751-784.

[55] J.S. Cintra, Jr., C.L. Tucker, III, Orthotropic closure approximations for flow-induced fiber orientation, Journal of Rheology 39(6) (1995) 1095-1122.

[56] V. Verleye, A. Couniot, F. Dupret, Numerical prediction of fibre orientation in complex injection-moulded parts, WIT Transactions on Engineering Sciences 4 (1970).

[57] I. Doghri, L. Tinel, Micromechanics of inelastic composites with misaligned inclusions: Numerical treatment of orientation, Computer Methods in Applied Mechanics and Engineering 195(13) (2006) 1387-1406.

[58] D.H. Chung, T.H. Kwon, Improved model of orthotropic closure approximation for flow induced fiber orientation, Polymer Composites 22(5) (2001) 636-649.

[59] M. Hajikazemi, L.N. McCartney, H. Ahmadi, W. Van Paepegem, Variational analysis of cracking in general composite laminates subject to triaxial and bending loads, Composite Structures 239 (2020) 111993.

[60] A. Schmitz, P. Horst, A finite element unit-cell method for homogenised mechanical properties of heterogeneous plates, Composites Part A: Applied Science and Manufacturing 61 (2014) 23-32.

[61] B. Piezel, B.C.N. Mercatoris, W. Trabelsi, L. Laiarinandrasana, A. Thionnet, T.J. Massart, Bending effect on the risk for delamination at the reinforcement/matrix interface of 3D woven fabric composite using a shell-like RVE, Composite Structures 94(8) (2012) 2343-2357.

[62] T.D. Dinh, D. Garoz, M. Hajikazemi, W. Van Paepegem, Mesoscale analysis of ply-cracked composite laminates under in-plane and flexural thermo-mechanical loading, Composites Science and Technology 175 (2019) 111-121.

[63] S. Fillep, J. Mergheim, P. Steinmann, Towards an efficient two-scale approach to model technical textiles, Computational Mechanics 59(3) (2017) 385-401.

[64] N.D. Barulich, L.A. Godoy, P.M. Dardati, Evaluation of cross-ply laminate stiffness with a non-uniform distribution of transverse matrix cracks by means of a computational meso-mechanic model, Composite Structures 185 (2018) 561-572.

[65] N. Mentges, B. Dashtbozorg, S.M. Mirkhalaf, A micromechanics-based artificial neural networks model for elastic properties of short fiber composites, Composites Part B: Engineering 213 (2021) 108736.

[66] L.N. McCartney, 7 - Applications of Maxwell's methodology to the prediction of the effective properties of composite materials, in: W. Van Paepegem (Ed.), Multi-Scale Continuum Mechanics Modelling of Fibre-Reinforced Polymer Composites, Woodhead Publishing2021, pp. 179-216.

[67] A. Digimat, Software for the Linear and Nonlinear Multi-Scale Modeling of Heterogeneous Materials; e-Xstream Engineering: Louvain-la-Neuve, Belgium, 2011.